Journal of Materials Chemistry B

Accepted Manuscript

ROYAL SOCIETY OF CHEMISTRY

www.rsc.org/materialsB

Journal Name

RSCPublishing

ARTICLE

Synthesis of Water Well-dispersed PEGylated Iron Oxide Nanoparticle for MR/Optical Lymph Node Imaging

Cite this: DOI: 10.1039/xoxxooooox

Received ooth January 2012,

Accepted ooth January 2012

DOI: 10.1039/xoxxooooox

www.rsc.org/

Kyung Mo Yang,[a] Hong Il Cho,[b] Hyuck Jae Choi,*[b,c] and Yuanzhe Piao*[a,d]

: We reported the synthesis of highly water-stable iron oxide nanoparticles by a simple one-pot reaction. Non-toxic polyethylene glycol MW 600 (PEG) acted as a solvent, capping agent and reducing agent in the synthesis of iron oxide nanoparticles. As a result of the synthesis, PEGylated small-size (4.2 ± 0.39 nm average diameter and 7.2 ± 1.9 nm hydrodynamic sizes measuring by DLS) iron oxide nanoparticles were obtained (USPIO), which show great colloidal stability in water and tolerate high salt concentration (0.75 M sodium chloride) and a wide pH range of 4 to 12. Oxidation of PEG was observed during the synthesis of iron oxide nanoparticles, which makes USPIO easy to functionalize with other molecules. Functionalization of the USPIO surface with Fluorescein isothiocyanate (FITC) was conduct for investigating the possibility to multimodal imaging. Also cytotoxicity test and lymph node imaging were performed by using the FITC labelled USPIO (FITC@USPIO). According to these results, the stable water dispersed USPIO and FITC@USPIO are expected to apply for multimodal *in vivo* imaging.

Introduction

With the advance of nanotechnology, the use of nanoparticles for biomedical applications has received much attention.[1, 2] Especially, magnetic iron oxide nanoparticles attracted great research interests in the development of multifunctional imaging agents since magnetic iron oxide nanoparticles are considered nontoxic, and can be used as MR contrast agents naturally through the production of spin-spin relaxation effects inducing T1 and T2 relaxation time changes.[3-6]

There are many routes for synthesizing iron oxide nanoparticles. Among them, co-precipitation method is one of the most important and widely used method,[7] which represented by Feridex® as commercialized iron oxide based MR imaging contrast agents. Although co-precipitation method has many advantages like easy to synthesis and functionalize,[8] the synthesized iron oxide nanoparticles using this method have irregular morphology and broad size distribution.[9] To solve these problems, many research groups have developed other synthetic methods such as micro emulsion process,[10] sol-gel process including hydrolytic routes and non-hydrolytic routes.[11-14]

Nowadays, thermal decomposition method has been taking center stage in the synthesis of monodisperse iron oxide nanoparticles.[15] The produced iron oxide nanoparticles using this powerful method have regular shape, high uniformity, and high crystallinity.[16, 17]

However, since the synthesis of iron oxide nanoparticles using thermal decomposition method is performed in the presence of long-chain surfactants such as fatty acid or fatty amine, the synthesized nanoparticles have hydrophobic surface inevitably and cannot be used for biomedical application directly. Most approaches to solve this problem are rely on ligand exchange process which include exchange of absorbed surfactant with biocompatible hydrophilic molecules having higher affinity groups (phosphate group[18, 19] or multidentate catechol[20]) for iron oxide surface than pre-chemisorbed long-chain organic surfactants. A major difficulty encountered in the ligand exchange process is hydrodynamic size increase problem and it limits the long term stability when dispersed in physiological medium.[21]

Since the stability of iron oxide nanoparticles dispersed in physiological medium is influenced dominantly by molecules absorbed on the surface of nanoparticles, the selection of the surface molecules for iron oxide nanoparticles is important for biological uses whether the ligand exchange process is necessary or not. Hence the surface molecules must fulfil several things including good stability in physiological buffer, biocompatibility, and preventing the nonspecific interaction with a cell in biomedical applications.[22, 23] Various types of organic or inorganic materials can be utilized for the surface

molecules of iron oxide nanoparticles. [24, 25, 26] In particular, low molecular weight PEG has been paid a lot of attention as a candidate organic surface molecule in biomedical perspective. PEG anchored on the surface of nanoparticles leads to reduce nonspecific binding with a cell and improve viability and stability by retaining a helical conformation of the crystalline state in water.[27] For this reason, synthesis of PEGylated monodisperse iron oxide nanoparticles has important meaning for real biomedical application. Hence, there are already a lot of research papers about PEGylation of the iron oxide nanoparticles.[28] However, most ways were relying on the post-synthetic treatment after synthesis of iron oxide nanoparticles, which were time consuming complex processes. There is need to develop simple and efficient way for synthesizing PEGylated iron oxide nanoparticles, since the route that allows for the synthesis PEGylated iron oxide nanoparticles in a single step has not so far been devised.

In this study, ultra small PEGylated iron oxide nanoparticles (USPIO) were synthesized in a simple one-pot reaction using iron nitrate as iron precursor in the presence of PEG. During the synthesis, oxidation of PEG was occurred in the synthesis. As a result of the oxidation of PEG, carboxylic acid group are arisen, consequently control the particle growth and prevent aggregation effectively, which was confirmed by using FT-IR. The morphology of the iron oxide nanoparticles was studied using TEM. DLS measurements show that particles were well-dispersed in water. The stability tests of the USPIO show high stability of the USPIO even at high salt concentration and broad range of pH. Encouraged by the evolution of surface functional group and high stability in water, we try to develop multimodal imaging agents using the USPIO. The USPIO were amine functionalized using dicyclohexylcarbodiimide / N-hydroxysuccinimide (DCC / NHS) coupling. Subsequently, FITC@USPIO were synthesized via the reaction of a primary amine with an isothiocyanate and their cytotoxicity test was performed. The FITC@USPIO show low toxicity. Furthermore, multimodal lymph node imaging using FITC@USPIO was performed to investigate the possibility to use for *in vivo* applications. These results demonstrate that the simply synthesized iron oxide nanoparticles have potential possibilities to use for *in vivo* multimodal imaging.

Experimental

Chemicals and materials

Ferric nitrate nonahydrate, poly (ethylene glycol) 600 (PEG), diethyl ether, dimethylformamide (DMF), chloroform, sodium hydroxide (NaOH) and hydrochloric acid (HCl), sodium bicarbonate, chloroform, dimethyl sulfoxide (DMSO) were acquired from Samchun Chemical. 0.01M phosphate buffered saline (PBS, pH 7.4) and phenolphthalein were obtained from Sigma-Aldrich. 0.1 M standardized hydrochloric acid solution was obtained from Fluka. All reagents were used as received and aqueous solutions were prepared using high purity deionized water (18.2 MΩ).

Characterization

Powder X-ray diffraction (XRD) patterns of the USPIO were obtained from Rigaku Dmax 2500 diffractometer with Cu Kα radiation (λ = 1.5406 Å) at 40 kV and 100 mA. Transmission electron microscopic (TEM) and high resolution TEM (HR-TEM) images were collected by JEM-3010 (JEOL) at an accelerating voltage of 300 kV. Size and size distribution of samples dispersed in water were estimated by Zetasizer Nano ZS equipped with a laser operating at 633 nm He-Ne laser with back scattering detector at 173° (Malvern). Fluorescence excitation and emission spectra were obtained by FluoroMate FS-2 (Scinco). FT-IR spectra were collected with Nicolet 6700 using Attenuated total reflectance (ATR) mode (Thermo electron corp.). Thermo gravimetric analysis was conducted using TGA / DSC 1-Thermo gravimetric analyzer (Mettler-Tolledo). Inductively coupled plasma-emission spectrometer (Shimadzu, JP / ICPS-7500) was used to quantify the iron concentration of the nanoparticle dispersed solutions.

Cell culture and viability test

Human ovarian cancer cells (SKOV3) were grown on glass coverslips in McCoy's 5A medium supplemented with 10% (v/v) fetal bovine serum (FBS), 100 units/mL penicillin, and 100 μL/mL streptomycin in an atmosphere of 95% humidified air and 5% CO_2 at 37 °C until the exponential phase was attained. Cultures that were 70-85% confluent were transferred to fresh culture dishes for 24 hours, after which the medium was replaced by medium without FBS to avoid non-specific binding of FITC@USPIO to serum albumin. The cells were next incubated with 50 μg Fe / mL FITC@USPIO in the presence of 1.5 μg / mL poly-L-lysine (PLL) (Sigma, St Louis, MO) for 24 hours.

The viability and proliferation capacity of such cells were evaluated using 3-[4, 5-dimethylthial-zol-2-yl]-2, 5-diphenyltetrazolium bromide (MTT, Sigma) assay. SKOV3 cells were seeded into 96 well plates at a density of 1×10^4 cells per well in 200 μL of media and grown overnight. The cells were then incubated with different concentrations of FITC@USPIO (0, 3, 6.125, 12.25, 25, 50, 100 μg Fe / mL) for 24 hrs. Following incubation, cells were incubated in media containing of 0.1 mg/mL of MTT for 1hr. Thereafter, MTT solutions were removed, and precipitated violet crystals were dissolved in 200 μL of DMSO.

Animal and specimen preparation

Female BALB/c nude mice aged 6-8 weeks were used in this study. The mice were anesthetized prior to MR and fluorescence imaging. All animal experiments were performed under sterile conditions, and with the approval of the Animal Care and Use Committee (ACUC) of our institution. The mice were euthanized with 1.5% (v/v) isoflurane in a 1:2 mixture of O_2:N_2O (v/v) on the day after imaging.

In Vitro MR imaging

The transverse relaxation rate R2 was assessed using multiecho sequences with spin-echo readout. The sequence parameters were as follows: TR = 3000 milliseconds, bandwidth = 250 Hz, FOV = 192 × 192 mm^2, matrix size = 192 × 144 mm, slice thickness = 4 mm. For these field strengths the TE used for calculation of the relativity values was varied in 32 equidistant steps between 16 milliseconds and 512 milliseconds.

Confirmation of R2 relaxation rate at higher concentrations of FITC@USPIO was achieved with TE times between 8 milliseconds and 256. Considering a mono-exponential decay, the signal intensity S (TE) is related to the TE according to the following equation.

$$S(TE) = A1 \cdot \exp(-R2 \cdot TE) + A2$$

In this regression, A1 refers to the equilibrium magnetization prior to sequence repetition, whereas A2 refers to the level of the noise. The transverse relaxation rate was determined by extrapolating the relaxation rate values of the measured samples.

Fluorescence imaging

In vivo fluorescence images were obtained with a fluorescence imaging system at an excitation wavelength of 480 nm (OptixMX3 / Optical Molecular Imaging System, Advanced Research Technologies, Canada) after injection of FITC@USPIO for 20 min.

In Vivo MR imaging

In vivo animal images were obtained using a 9.4T / 160mm animal MRI system (Agilent Technologies, Santa Clara, CA, USA). Radiofrequency excitation and signal detection were accomplished with a 40 mm millipede volume coil. The coronal imaging protocol included a Spoiled Gradient Recalled Echo (SPGR) [TR=300 ms; TE=4.58 ms; field of view, FOV=40 × 30 mm; matrix size = 256 × 256; and slice thickness=1mm (no gap)].

Synthesis of USPIO

We prepared iron oxide nanoparticles using ferric nitrate as precursor in PEG medium. To prepare 4.2 ± 0.39 nm iron oxide nanoparticles (TEM observation), 0.404 g (1 mmol) of ferric nitrate nonahydrate were mixed with 12 g (20 mmol) of PEG to get transparent red solution. The resulting mixture was heated to 80 °C with a constant heating rate of 10 °C / min and kept at that temperature for 0.5 hr. Subsequently, the mixture was heated to 265 °C with a constant heating rate of 3 °C / min and held at that temperature for 0.5 hr. Synthesis was proceeded under low pressure (-76 cmHg) to remove generated H_2O vapour as presented in PEG and precursor until 160 °C using shrink line. Then, nitrogen was purged into reactor until the reaction was ended. During this process, the initial transparent red solution was gradually changed to brown when the temperature was above 140 °C. Brownish black solution was obtained at the end of the reaction, indicating the formation of iron oxide nanoparticles. Subsequently, the resulting solution was cooled to room temperature with removal of the heat source. 1: 5 ethanol / ether mixture was added to the solution and the nanoparticles were separated by centrifugation.

Synthesis of FITC@USPIO

The USPIO were functionalized with 1, 2-ethylenediamine. To prepare amine functionalized USPIO, 6 g of the as-synthesized solutions were washed with ethanol, diethyl ether mixture twice by centrifugation and re-disperse in 15 mL of DMF. Then, 300 µl of DCC (10 mg in 1 ml DMF) and NHS (5.5 mg in 1 mL DMF) solutions were added and stirred at R.T for another 10 min. Then, 50 µl of 1, 2-ethylenediamine was dropped into the solution. After stirring for 6 hr, 1:5 ethanol / ether mixture was added to the solution and the nanoparticles were separated by centrifugation at 8000 rpm to remove unreacted molecules and DCU (dicyclohexylurea). The washing process was repeated for several times. The amine functionalized iron oxide nanoparticles were re-dispersed in 15 mL of 0.01M sodium bicarbonate buffer solutions with pH 9.5 for further reaction with fluorescent dye. Then, FITC@USPIO was synthesized by adding FITC (5 mg in 1 mL DMSO) to the solutions. After stirring for 6 hr, the nanoparticles were washed by the same process. The separated nanoparticles were re-disperse in 0.01 M PBS pH 7.4 buffer, then the product was further purified by dialysis against 0.01 M PBS pH 7.4 buffer using tubing with a 12,000-14,000 MW cut-off (Zellu Trans, Roth (Germany)).

Results and discussion

Synthesis of iron oxide nanoparticles

In this study, ultra small PEGylated Iron oxide nanoparticles (USPIO) were synthesized using ferric nitrate as precursor in

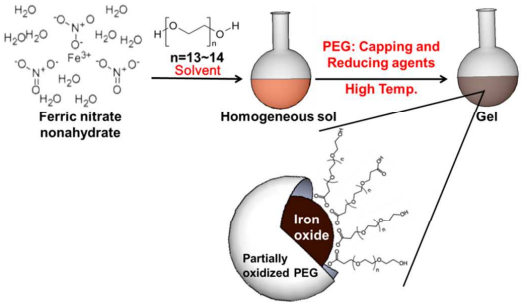

Scheme 1 Schematic illustration of the synthesis of iron oxide nanoparticles

the presence of PEG as described in Scheme 1. The shape and size of the USPIO were observed by using TEM. Representative TEM images of USPIO were shown in Fig 1 (A, B). Fig 1C is a size distribution histogram of the randomly selected 100 nanoparticles. From the TEM observation, USPIO have an average diameter of 4.2 ± 0.39 nm. Hydrodynamic size and size distribution of the USPIO were measured by using DLS. Hydrodynamic size of the USPIO dispersed in water was measured to be 7.2 ± 1.9 nm as shown in Fig 1D. The TEM and DLS measurements suggest the USPIO have narrow size distribution and well-dispersed in water.

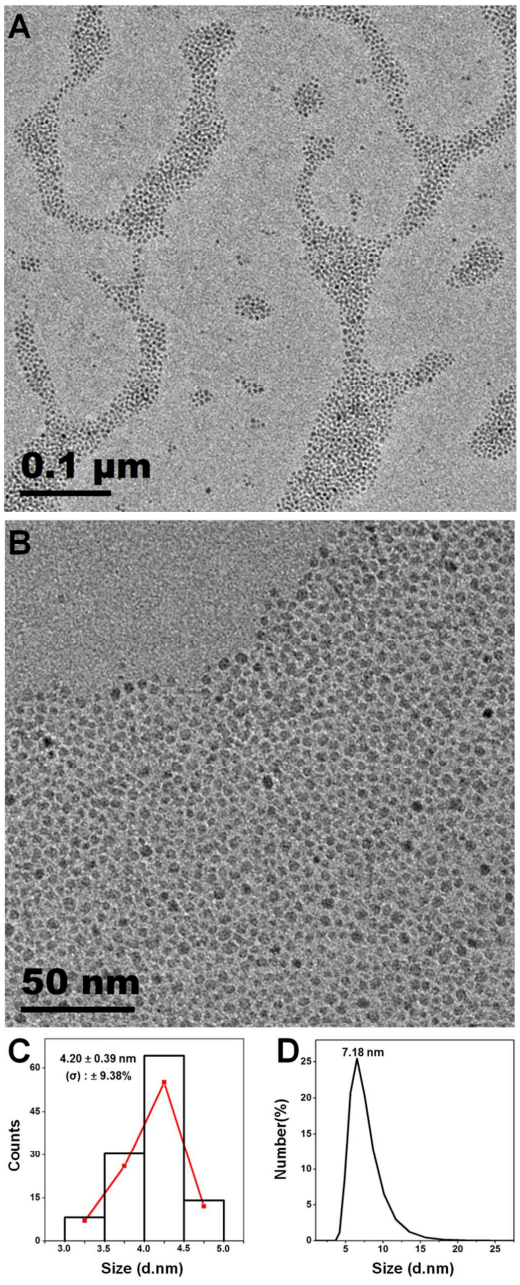

Fig 2 Representative TEM images of USPIO (A, B). The size distribution histogram of USPIO in TEM image (C). Hydrodynamic size (size distribution by number) of the USPIO (D).

Because the formation of iron oxide nanoparticles in our synthesis was based on the hydrolysis and thermal decomposition of iron nitrate nonahydrate,[29] generated H_2O as by-products would be expected to influence the growth of the

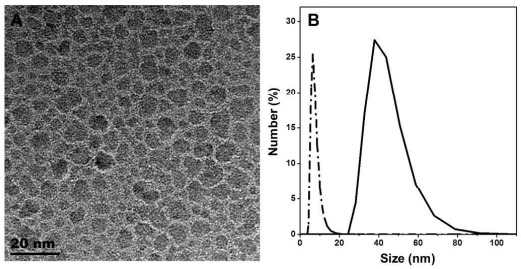

Fig 1 TEM image (A) and hydrodynamic size distribution of the synthesized iron oxide nanoparticles (B) without removal of water vapour.

iron oxide nanoparticles. To investigate the effect of H_2O generated in reaction, synthesis of iron oxide nanoparticles was performed under normal pressure. Increases of the hydrodynamic size was observed and eventually significant

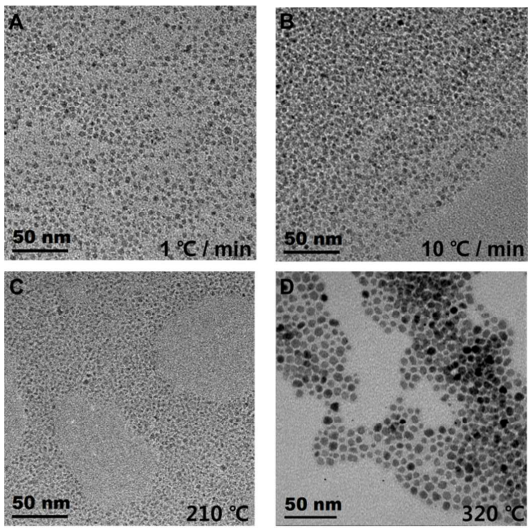

Fig 3 TEM images of the iron oxide nanoparticles with different preparation conditions ; heating rate of (A) 1°C / min and (B) 10°C / min ; aging temperature of (C) 210 °C and (D) 320 °C

agglomeration was occurred as a result of the accelerating the hydrolysis of the iron nitrate by H_2O (Fig 2B).[30]

Furthermore, we tried to control the size of the iron oxide nanoparticles by varying the heating rates and aging temperature. There are no significant changes in size and shape, when varying the heating rates (Fig 3A, B). Slight size changes of nanoparticles were carried out by varying the aging

temperature (Fig 3 C, D). TEM image shows that the size of the iron oxide nanoparticles is significantly decreased with an aging temperature of 210 °C. The nanoparticles show low stability and crystallinity (Fig S1). In an aging temperature of 320 °C, increasing of the nanoparticle size was observed in TEM images. From experimental results, 265 °C was chosen as optimized aging temperature.

Crystal structure study of the USPIO

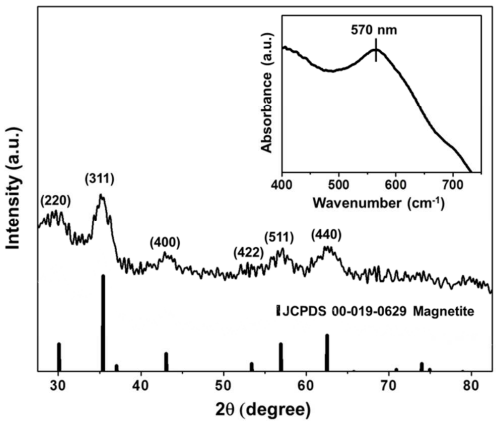

Fig 4 XRD pattern of the USPIO. Inset is the FT-IR spectra in 500 - 750 cm^{-1} ranges.

XRD measurements were conducted to confirm the crystal structure of USPIO. XRD Patterns of the USPIO are summarized in Fig 4. The peaks were indexed with (JCPDS # 00-019-0629). (200), (311), (400), (422), (511) and (440) were revealed in the XRD pattern, though the (111) peak could not be distinguishable because of the overlap pattern of surface organic molecule, PEG.[31] The crystalline size of the USPIO was calculated by fitting the data to a Gaussian distribution and applying Debye-Scherrer equation on the (440) diffraction peak. In this study, we used the value K=0.9, λ=1.54 Å. The calculated crystal size is 4.09 nm and that is slightly smaller than TEM observation, which corroborate with Fig S2. The Fig S2 is image of HRTEM and the inset of Fig S2 is fast Fourier transform (FFT) pattern of the selected region of HRTEM image indicating crystal structure of the USPIO. FT-IR measurement was conducted for more accurate investigation of crystal structure, because it is hard to distinguish between magnetite and maghemite in XRD patterns. The lattice adsorption band from FT-IR spectra of the USPIO is appeared one peak at about 570 cm^{-1} with broad shoulder up to 750 cm^{-1} shown in inset of the Fig 4 indicate that the USPIO are predominately magnetite although they have a little oxidized layer.[32] From the crystal structure of the USPIO, we confirmed that the reduction of ferric ions to ferrous ions is existed in the reaction. Polyol reduction at high temperature may be a possible route[16], although the mechanism leading to magnetite under this reaction condition is not clear. Furthermore, the oxidation of PEG could be expected, in this perspective. This assumption is corroborated with the explanation given in FT-IR study.

Surface studies of the USPIO

There are early studies of the interaction between polymer and surface of iron oxide nanoparticles. Zhang et al reported the chemisorption of polymethacrylic acid to the surface of Fe_3O_4 nanoparticles via coordination linkages between the carboxyl groups and Fe.[33] To study the interaction between PEG and iron oxide, we conducted TGA and FT-IR study. TGA measurement of the USPIO was carried out from 25 °C to 700 °C with a heating rate of 10 °C / min in air condition. Thermal degradation of the USPIO is derived from the thermal

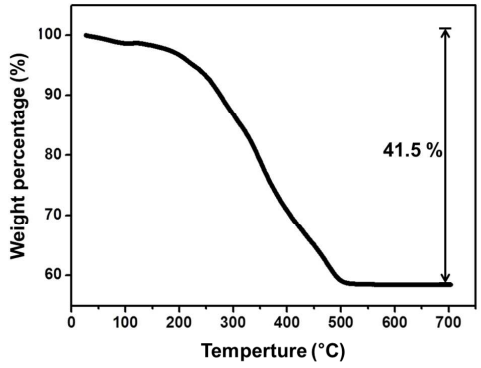

Fig 5. TGA curve of the as-synthesized USPIO

degradation of the surface organic molecules, which densely cover USPIO with 41.5 weight percentage (Fig 5). The surface density of the conjugated PEG was calculated to be 2.6 ± 0.2 (ea. / nm^2) based on the TGA result with basic assumption. Detailed calculations of USPIO were shown in Table S1. To investigate a better understanding the covered organic molecules, we conducted FT-IR study since FT-IR study is an appropriate technique to establish the attachment of polymer onto the surface of the USPIO. In FT-IR study, we could confirm the surface of the USPIO covered by the oxidized PEG. The FT-IR spectra of PEG and USPIO are shown in Fig 6A and B. Characteristic peaks were assigned, associated with PEG. The peaks at 1100 and 2860 cm^{-1} were corresponded to stretching vibration of C-O-C and symmetric stretching vibration of sp^3 C–H. Stretching vibration of hydrogen bonded OH^- was ascribed as 3460 cm^{-1}, although small peak shift of the hydroxyl group to lower wavenumber and broadening of peak were observed in the case of the USPIO. The peak at 1420 cm^{-1} is corresponded to the symmetric stretching vibrations of C=O-

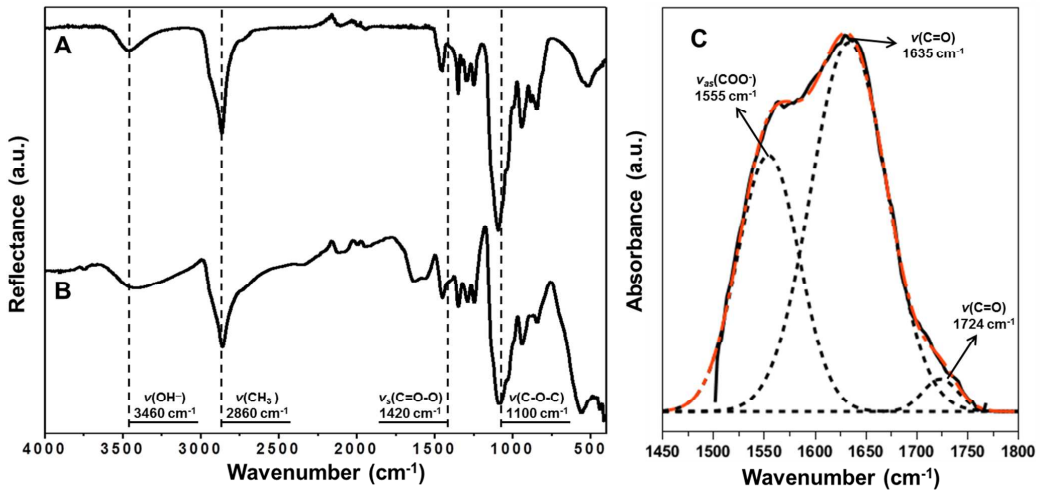

Fig 6 FT-IR spectra of PEG (A) and USPIO (B). (C) is a Gaussian fitted spectra of the as-synthesized USPIO in 1450 - 1800 cm^{-1} ranges.

O, which hidden by the bending vibration of CH_2. Furthermore, peaks were related with carbonyl group observed in the spectra by applying the Gaussian fitting in 1450-1800 cm^{-1} ranges of the USPIO as shown in Fig 6C. The peak at 1555 cm^{-1} was corresponded to asymmetric stretching vibration of the C=O-O. The two peaks at 1724 and 1635 cm^{-1} were identified as corresponding to two distinct stretching vibration of C=O. The peak appeared at 1635 cm^{-1}, is corresponded to the carboxylate group interacts with the iron on the SPION surface,[34] while the peak appeared at 1724 cm^{-1} is related to the free carboxylic acid.[35] The result suggests the presence of small portion of free carboxyl groups in the USPIO. Oxidation of PEG can be considered based on the evolution of nitric acid during the synthesis.[36] The oxidation of PEG was demonstrated by S. Joshi et al. They suggested possible mechanism of the oxidation of any glycol on heating. Any glycol on heating, terminal hydroxyl group of PEG is converted into aldehyde group. As a result of the chelation of cationic ion with two aldehydic oxygen atoms and etheric oxygen atom, they forms intermediate complex. Further oxidation of aldehyde groups to carboxylic acid groups occurred by increasing temperature in the presence of intermediately formed nitric acid.[37] To quantifying the carboxylic acid groups conjugated onto USPIO as a result of oxidation of PEG, we used the base-acid back-titration methods. The 100 mg of washed USPIO was dispersed in 10 ml of 0.1 M NaOH solution to ensure that the entire carboxylic acid group was reacted with NaOH. In order to complete the base-acid reaction, the solutions were sonicated for 30 min. To avoid the confusion in color change, 2 L of distilled water was added to the prepared solution, and then 3 drops of 1% phenolphthalein solution was added to the solution as pH-indicator. The back-titration was complete by titrating the unreacted base in solutions with standardized 0.1 M HCl to the solutions. The percentage of the oxidized PEG was calculated to be 18.7%. The result was summarized in Table S2.

Stability test of the USPIO

Stability of the nanoparticles is the most important property for biological and medical applications. Moreover stability of the nanoparticles can be related to surface's molecules directly as we mentioned above. Especially, PEG is attracted much attention as surface molecules from there biocompatibility with colloidal stability enhancement properties due to steric

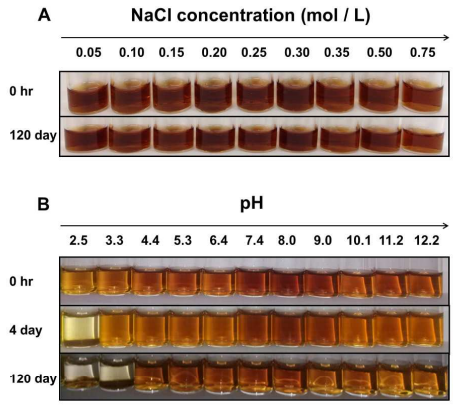

Fig 7 (A) Photograph of the USPIO dispersed in various NaCl concentration solutions. (B) Photograph of the USPIO dispersed in various pH conditions.

repulsion of the PEG chains on the particle surface. In this study, the surface of USPIO is covered by the oxidized PEG in synthetic procedure as we confirmed, so it could be expected a good colloidal stabilities. The colloidal stability of the as-synthesized USPIO was tested in 0.01 M PBS pH 7.4 buffer containing 0.05 M to 0.75 M NaCl solutions at final Fe concentrations of 150 μg / ml. There are no precipitations or aggregations observed over 4 month (Fig 7A). This high stability of the USPIO came from the PEG, which were densely covered the iron oxide nanoparticle surface. The stability of the dispersed nanoparticles is strongly depends on the net surface charge which is affected by pH. Zeta potential in 0.01M PBS media at broad ranges of pH of the USPIO were plotted in Fig S3. The USPIO were well dispersed in broad ranges of pH (from pH 4 to 12) solution over 4 month while USPIO dispersed in pH 2.5 solution were tended to form a turbid dispersion and completely precipitated over 4 days. USPIO dispersed in pH 3.3 solution were precipitated completely over 4 month as shown in Fig 7B. Furthermore, the as-synthesized USPIO could also be well dispersed in some organic solvents as shown in Fig S4. From the results mentioned above, we confirmed that the USPIO are very stable over broad ranges pH and salt concentration because of steric stabilization and electrostatic repulsion of PEG on the surface of the USPIO.

Functionalization of the USPIO

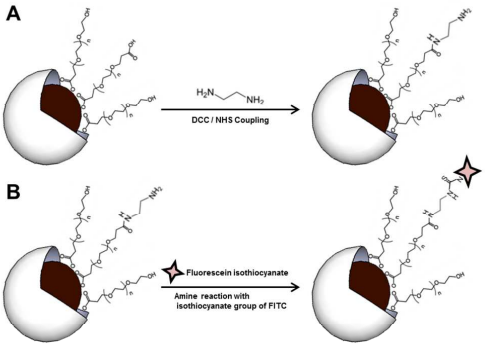

Scheme 2 Schematic illustration of functionalization of the USPIO

Especially, multimodal imaging techniques based on the multimodal imaging agents have attracted much attention nowadays. In this work, functionalization of the USPIO was conducted for multimodal imaging, thanks to the generation of surface free carboxylic acid group of PEG on the surface of USPIO as we described above. Functionalization steps were divided into two steps (Scheme 2). First, amine functionalization of the terminal carboxylic acid group was conducted via DCC coupling (Scheme 2A). Second, FITC were attached to the amine functionalized iron oxide nanoparticle surface via reaction of isothiocyanate groups with surface's amine groups (Scheme 2B). Amine functionalization of the surface of USPIO was confirmed by FT-IR spectra shown in Fig S4. There are decreasing of the stretching vibration peak intensity of OH^-, that was appeared at 3460 cm^{-1} and arising of a broad peak located in 2900-3600 cm^{-1} ranges, which may be contributed by the stretching vibration of primary, secondary NH group and OH^-. The peak of 1022 cm^{-1} was corresponded to the stretching vibration of C-N group. The Gaussian fitted FT-IR spectra in 1450-1700 cm^{-1} ranges, show two peaks of 1592 cm^{-1} and 1645 cm^{-1} were correspond to the bending vibration of primary NH group and stretching vibration of C=O group.

Emission and excitation spectra of FITC@USPIO are shown in Fig 8. The fluorescent spectra indicated that FITC molecules were attached to the iron oxide nanoparticles successfully. Also

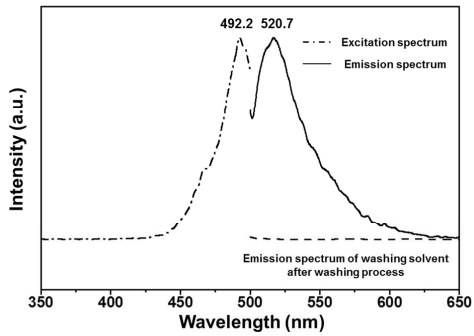

Fig 8 Excitation and emission spectra of FITC@USPIO.

DLS data show that agglomeration was not occurred during the functionalization of the USPIO (Fig S6). The concentration of FITC on the surface of USPIO was calculated by substituting the standard curve of FITC. The calculated amount of FITC molecules is 20.7 ± 0.70 ea. for each USPIO. Standard curve of FITC at 493 nm, and absorbance of FITC@USPIO in various concentrations in 400 ~ 500 nm ranges were plotted in Fig S7. Detailed calculations were summarized in Table S3. From these FT-IR and PL spectra, we confirmed that the functionalization of the USPIO with FITC was done successfully.

Cytotoxicity and in vitro Study

Prior to adopt the FITC@USPIO in lymph node imaging, the cytotoxicity, relaxivity and biodistribution study of FITC@USPIO were conducted. The cytotoxicity of the FITC@USPIO was measured using SKOV3 cell by MTT analysis at different concentrations (from 0 to 100 μg Fe / ml). MTT assay revealed that cell viability of SKOV3 cell was not hindered after 24 hr incubation with FITC@USPIO up to concentration of 100 μg Fe / mL as shown in Fig 9.

Fig 10A show T2-weighted images with various concentration of Fe

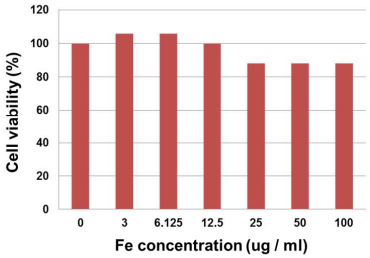

Fig 9 MTT assays of FITC@USPIO using SKOV3 cells after 24 hr incubation at 37 °C

(from 0.358 to 2.686 mM). The Fe concentrations of USPIO dispersed in solutions were quantified by ICP. More specifically, dispersions of USPIO in various concentrations were treated with concentrated HCl to complete the dissolving USPIO and quantified by ICP. The R2 relaxation rates of normal saline plotted against concentration of the FITC@USPIO are shown in Fig 10B. Higher concentrations of the FITC@USPIO resulted in higher R2 relaxation rates. To evaluate the contrast enhancement efficiency, specific relaxivity value (r2) was calculated. The calculated r2 was 27.5 $mM^{-1}s^{-1}$, which small r2 was derived from the small size of the iron oxide core with the organic molecules (FITC and oxidzed PEG) of FITC@USPIO.

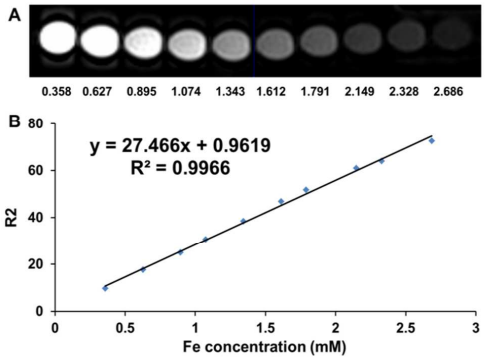

Fig 10 T2-weighted MRI images of various concentrations of FITC@USPIO (A) R2 relaxation rates as a function of iron concentration (mM) of FITC@USPIO dispersed in 0.01 M PBS pH 7.4 buffer (B)

Biodistribution study

We conducted the biodistribution study in the body to see main root of excretion of FITC@USPIO and dynamic change of FITC@USPIO in organs after venous injection. The FITC@USPIO dispersion (0.23 mg Fe /kg) was injected to tail vein of mouse after anesthesia. Serial coronal MR images were obtained prior to injection of FITC@USPIO and up to 1 day after injection (immediate, 1hour, 3 hours, and 1 day after injection). After intravenous injection of FITC@USPIO into the tail vein of mouse, enhancement was continued until 3 hours and the nanoparticles were accumulated in the liver, spleen, and kidney. After 24 h of injection, no contrast material was visualized in the kidney but contrast still remained in the liver and spleen as shown in Fig 11.

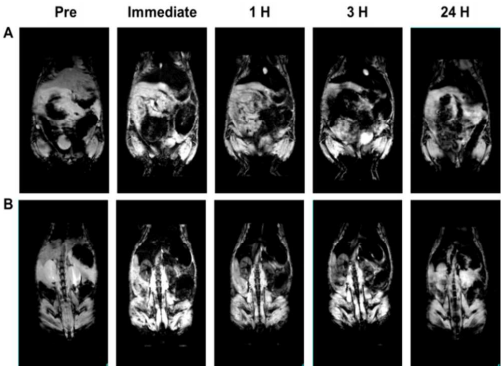

Fig 11 Serial T2* coronal MR imaging (A, B) of mouse after injection of FITC into the tail vein. Signal intensity of the spleen, kidney, and liver gradually decreased until 3 hours after FITC injection. After 24 hours after injection the signal intensity of the kidney became normal but those of the spleen and liver still remains decreased.

***In vivo* lymph node imaging**

For lymph node imaging, 100 μL solution of FITC@USPIO solution (4.5 mg Fe / ml) was intradermally injected into the tops of the feet of right hind legs. Twenty minutes after injection, the location of popliteal and inguinal lymph nodes were well visualized in optical imaging as shown in Fig 12A, which indicated by filled triangle and non-filled triangle. Furthermore, MR images were acquired 30 minutes after injection of FITC@USPIO. The location of the inguinal lymph node was determined by MR imaging (Fig 12B). After mice were euthanized by inhalation of pure CO_2, right inguinal lymph nodes were harvested. Transverse sections 4 μm in thickness were obtained and stained with Prussian blue to detect intracellular iron. In dissected lymph nodes, the FITC@USPIO was observed (Fig 12C). These areas corresponded to the location of hypo-intense regions on MR T2* images. Furthermore, a series of in vivo coronal and axial T2* MR images 30 min after injection of FITC@USPIO were taken for accurate confirmation of uptake of the FITC@USPIO in inguinal lymph node (Fig S8). The transportation of the FITC@USPIO to the lymph node was derived from the small size of the FITC@USPIO which was enough to drain into the lymphatic vessels and consequently flow into lymph node.

Formatted: Font: Times New Roman, 9 pt, Bold

From these results, FITC@USPIO show high possibilities to use for multimodal *in vivo* lymph node imaging.

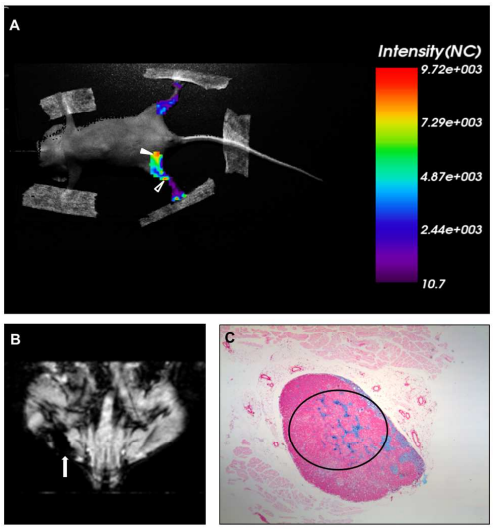

Fig 12 (A) *In vivo* optical images of a mouse 20 minutes and back after FITC@USPIO injection to the top of right hind leg. Inguinal and popliteal lymph nodes were indicated by filled and non-filled triangle. (B) *In vivo* T2* coronal MR imaging 30 minute after injection of FITC@USPIO. The white arrow indicates inguinal lymph node (C) Prussian blue stained section of dissected lymph node. The blue area in the circle indicated FITC@USPIO

Conclusions

In this study, the water well-dispersible USPIO were synthesized in PEG solution without additional surfactant, through simple one-pot polyol process. PEG was oxidized during the synthesis of the USPIO. As a result, adsorption of the oxidized PEG to iron oxide nanoparticles surface is observed with small portion of surface free carboxylic acid group, which allow easy functionalization with the optical imaging agents. 1, 2-ethylenediamine was introduced to the surface of iron oxide nanoparticles via DCC coupling. The resulting amine functionalized USPIO were conjugated with FITC through the reaction of isothiocyanate group with amine group at R.T. From the results of biological experiments including lymph node imaging using FITC@USPIO, the simply synthesized USPIO show great potentials to use for *in vivo* multimodal imaging.

Acknowledgements

Y.P. thanks the financial support by the Korea Healthcare Technology R&D Project, Ministry for Health, Welfare & Family Affairs, Republic of Korea (A092145). This work was also supported by the National Research Foundation of Korea (NRF) grant funded by the Korea government (MEST) (No. 2011-0001302 and 2011-0013169). The authors gratefully acknowledge technical support from Biomedical Imaging Infrastructure, Department of Radiology, Asan Medical Center.

Notes and references

[a] Graduate School of Convergence Science and Technology, Seoul National University, Seoul, 151-742, Republic of Korea
[b] Asan Institute for Life Sciences, University of Ulsan College of Medicine, Seoul, 138-736, Republic of Korea
[c] Department of Radiology, Asan Medical Center, University of Ulsan, Seoul 138-736, Republic of Korea
[d] Advanced Institutes of Convergence Technology, Suwon 443-270, Republic of Korea

† Footnotes should appear here. These might include comments relevant to but not central to the matter under discussion, limited experimental and spectral data, and crystallographic data.

Electronic Supplementary Information (ESI) available: [XRD pattern of the as-synthesized iron oxide nanoparticles at 210°C, HRTEM image and a FFT pattern of the USPIO, Zeta potential of the USPIO in various pH conditions, Photograph of dispersion of USPIO in various solvents, FT-IR spectra of the amine-functionalized USPIO and Gaussian fitted FT-IR spectra of the amine-functionalized USPIO in 1450 - 1700 cm^{-1} ranges, Hydrodynamic sizes of the USPIO and FITC@USPIO. Quantification of USPIO, Base-acid back titration results of USPIO, Standard curve of FITC at 493 nm and FITC@USPIO absorbance curve in 400 – 500 nm ranges, Quantification of FITC molecules conjugated onto each USPIO, The series of *in vivo* T2* coronal MR image and the series of *in vivo* T2* axial MR image of lymph node]. See DOI: 10.1039/b000000x/

1. R. Hao, R. Xing, Z. Xu, Y. Hou, S. Gao and S. Sun, *Adv. Mater.*, 2010, 22, 2729-2742.
2. M. C. Daniel and D. Astruc, *Chem Rev.*, 2004, 104, 293-346.
3. J. Kim, Y. Piao and T. Hyeon, *Chem. Soc. Rev.*, 2009, 38, 372-390.
4. B. J. Pichler, M. S. Judenhofer and H. F. Wehrl, *Eur. Radiol,.* 2008, 18, 1077-1086.
5. H. P. W. Schlemmer, B. J. Pichler, M. Schmand, Z. Burbar, C. Michel, R. Ladebeck, K. Jattke, D. Townsend, C. Nahmias, P. K. Jacob, W. D. Heiss and C. D. Claussen, *Radiology*, 2008, 248, 1028-1035.
6. W. de Heer, P. Milani and A. Chtelain, *Phys. Rev. Lett.*, 1990, 65, 488-491.
7. L. Babes, B. Denizot, G. Tanguy, J. J. L. Jeune and P. Jallet, *J. Colloid Interface Sci.*, 1999, 212, 474-482.
8. A. B. Bourlinos, A. Bakandritsos, V. Georgakilas and D. Petridis, *Chem. Mater.*, 2002, 14, 3226-3228.
9. N. Bao, L. Shen, Y. Wang, P. Padhan and A. Gupta, *J. Am. Chem. Soc.*, 2007, 129, 12374-12375.
10. S. Santra, R. Tapec, N. Theodoropoulou, J. Dobson, A. Hebard and W. Tan, *Langmuir*, 2001, 17.
11. A. M. G. Ennas, G. Piccaluga, D. Zedda, D. Gatteschi, C. Sangregorio, J. L. Stanger, G. Concas and G. Spano, *Chem. Mater.*, 1998, 10, 495-502.
12. M. Niederberger, *Acc. Chem. Res.*, 2007, 40, 793-800.
13. M. Niederberger, G. Garnweitner, N. Pinna and G. Neri, *Prog. Solid State Chem.*, 2005, 33, 59-70.
14. W. W. Yu, J. C. Falkner, C. T. Yavuz and V. L. Colvin, *Chem. Commun.*, 2004, 20, 2306-2307.
15. N. R. Jana, Y. F. Chen and X. G. Peng, *Chem. Mater.*, 2004, 16, 3931-3935.
16. S. H. Sun and H. Zeng, *J. Am. Chem. Soc.*, 2002, 124, 8204-8205.
17. J. Park, K. An, Y. Hwang, J. G. Park, H. J. Noh, J. Y. Kim, J. H. Park, N. M. Hwang and T. Hyeon, *Nat. Mater*, 2004, 3, 891-895.

18. U. I. Tromsdorf, O. T. Bruns, S. C. Salmen, U. Beisiegel and H. Weller, *Nano Lett*, 2009, 9, 4434-4440.
19. B. Dubertret, P. Skourides, D. J. Norris, V. Noireaux, A. H. Brivanlou and A. Libchaber, *Science*, 2002, 298, 1759-1762.
20. H. B. Na, G. Palui, J. T. Rosenberg, X. Ji, S. C. Grant and H. Mattoussi, *ACS nano*, 2012, 6, 389-399.
21. J. Xie, C. Xu, N. Kohler, Y. Hou and S. Sun, *Adv. Mater*, 2007, 19, 3163-3166.
22. Y. Piao, A. Burns, J. Kim, U. Wiesner and T. Hyeon, *Adv. Funct. Mater.*, 2008, 18, 3745-3758.
23. T. Neuberger, B. Schöpf, H. Hofmann, M. Hofmann and B. von Rechenberg, *J. Magn. Magn. Mater.*, 2005, 293, 483-496.
24. R. T. Swadeshmukul Santra, Nikoleta Theodoropoulou, JonDobsor, Arthur Hebard, and Weihong Tan, *Langmuir*, 2001, 17, 2900-2906
25. S. S. Jean-Francois Lutz, Ann Hoth, Lutz Kaufner, Ulrich Pison, and Regis Cartier, *Biomacromolecules*, 2006, 7, 3132 - 3138.
26. V. S. H. Ding, M. Agudelo, S. Pilakka-Kanthikeel, V. S. R. Atluri, A. Raymond, T. Samikkannu, M. P. Nair, *Nanotechnology*, 2014, 25, 055101.
27. J. H. Lee, H. B. Lee and J. D. Andrade, *Prog. Polym. Sci*, 1995, 20, 1043-1079.
28. X. H. Peng, X. Qian, H. Mao, A. Y. Wang, Z. Chen, S. Nie, D. M Shin, *Int. J. Nanomedicine*, 2008, 3, 311-321.
29. K. Wieczorek-Ciurowa and A. J. Kozak, *J. Therm. Anal. Calorim.*, 1999, 58, 647-651.
30. J. Ge, Y. Hu, M. Biasini, W. P. Beyermann and Y. Yin, *Angew. Chem. Int. Ed.*, 2007, 46, 4342-4345.
31. J. Lheritier, A. Chauvet and J. Masse, *Thermochim. Acta*, 1994, 241, 157-169.
32. J. M. G. c. T. J. Daou, G. Pourroy, S. Buathong, A. Derory, C. Ulhaq-Bouillet, B. Donnio, D. Guillon, and S. Begin-Colin, *Chem. Mater.*, 2008, 20, 5869-5875.
33. H. Zhang, R. Wang, G. Zhang and B. Yang, *Thin Solid Films*, 2003, 429, 167-173.
34. Q. J. Fengqin Hu, Yilin Li and Mingyuan Gao, *Nanotechnology*, 2011, 22, 245604.
35. T. B. Cecilia B. Mendive, Miguel A. Blesabd and and D. W. Bahnemanna, *Phys. Chem. Chem. Phys.*, 2006, 8, 3232-3247.
36. M. E. Naofumi Uekawa, Kazuyuky Kakegawa and Yoshinori Sasaki, *Phys. Chem. Chem. Phys*, 2000, 2, 5485-5490.
37. S. N. Rishikeshi, S. S. Joshi, M. K. Temgire and J. R. Bellare, *Dalton Trans.*, 2013, 42, 5430-5438.

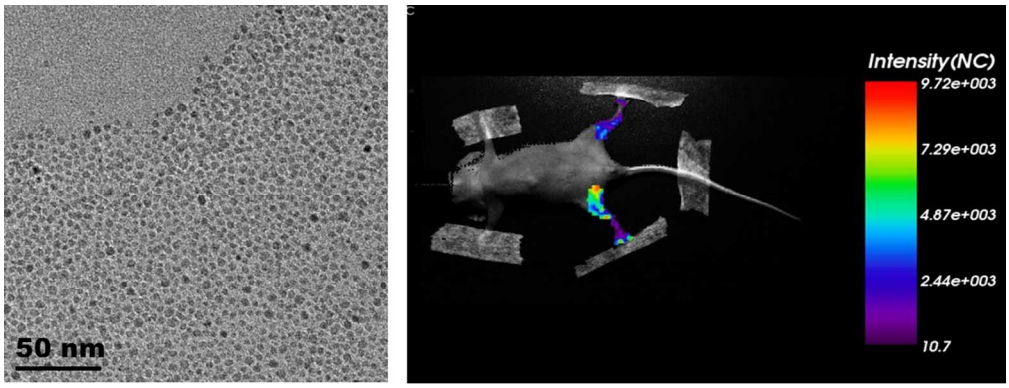

graphical abstract
318x120mm (96 x 96 DPI)